A cortical bone milling force model based on orthogonal cutting distribution method

Qi-Sen Chen[1] · Li Dai[1] · Yu Liu[1] · Qiu-Xiang Shi[1]

Abstract In orthopedic surgery, the bone milling force has attracted attention owing to its significant influence on bone cracks and the breaking of tools. It is necessary to build a milling force model to improve the process of bone milling. This paper proposes a cortical bone milling force model based on the orthogonal cutting distribution method (OCDM), explaining the effect of anisotropic bone materials on milling force. According to the model, the bone milling force could be represented by the equivalent effect of a transient cutting force in a rotating period, and the transient milling force could be calculated by the transient milling force coefficients, cutting thickness, and cutting width. Based on the OCDM, the change in transient cutting force coefficients during slotting can be described by using a quadratic polynomial. Subsequently, the force model is updated for robotic bone milling, considering the low stiffness of the robot arm. Next, an experimental platform for robotic bone milling is built to simulate the milling process in clinical operation, and the machining signal is employed to calculate the milling force. Finally, according to the experimental result, the rationality of the force model is verified by the contrast between the measured and predicted forces. The milling force model can satisfy the accuracy requirement for predicting the milling force in the different processing directions, and it could promote the development of force control in orthopedic surgery.

1 Introduction

In knee arthroplasty and bone tumor resection, it is of great significance to study the influences of feed direction and bone material properties on the cutting force for the development of medical robots. The modeling of bone cutting force has been recognized as a difficult problem, considering the effects of feed direction and bone material characteristics [1–3]. A large cutting force tends to lead to bone cracks and breaking of tools during the operation, which should not occur in orthopedic surgery [4–7]. The tight link between cutting force and bone crack has been verified in bone milling and orthogonal cutting [8, 9].

The bone cutting force is related to the bone material characteristics and bone processing direction. The different relative positions of the osteon orientation and machining direction make the cutting force modeling complicated [10–14]. Although the cutting process is performed along a specified direction, the inhomogeneous bone material would also intensify the fluctuation of the cutting force. Compared with bone milling force modeling, drilling force modeling is more common in bone cutting force modeling. For a long time, research on the modeling of bone-cutting force has mainly focused on the drilling force model. Firstly, Lee et al. [15] systematically put forward the mechanistic model of force and torque during bone drilling, considering the effect of drill-bit geometry and cutting parameters. Afterwards, Sui et al. [16] improved the bone drilling force model with an experimental validation and divided the cutting action at the drill point into the three regions: the cutting lips and the outer and inner portions of

✉ Yu Liu
yuliu@me.neu.edu.cn

1 School of Mechanical Engineering and Automation, Northeastern University, Shenyang 110819, People's Republic of China

the chisel edge. For simulating the bone material characteristics, the finite element modeling method of the drilling force is extensively employed during the bone machining process. Lughmani et al. [17] developed a 3D Lagrangian finite element model to predict the thrust forces and the torques, simplifying the bone samples into elastic-plastic materials using the Hill's potential theory for anisotropic materials.

The bone drilling force model cannot be applied directly to calculating the milling force because drilling is different from milling operations. Drilling is similar to one-dimensional processing, while milling is equivalent to two-dimensional machining. Meanwhile, there have been some exploratory studies on milling force modeling during the bone cutting process. Arbabtafti et al. [18] presented a novel modeling method of milling force by using the voxel principle to simulate the virtual bone and removed chips, which was only suitable for the spherical cutting burr in robot-assisted arthroplasty. Furthermore, Al-Abdullah et al. [19] also developed, by using artificial neural networks, a force and temperature model of bone milling aimed at the spherical burr.

The above milling force models are not suitable for end mills because the geometric shapes of spherical cutting burrs are very different from those of end milling cutters. Liao et al. [20] proposed a dynamic force model of bone milling for end mills based on the cutting stress of bone materials. For engineers or doctors, it is difficult to apply the cutting stress model to the force control of robotic orthopaedic surgery, as there are numerous parameters to be determined and complex theoretical calculations in the model.

Although bone cutting force modeling has been studied, the relationship between the milling force in different feed directions and the anisotropy of bone materials has not been reasonably explained. The drilling force models are different from the milling models owing to the machining principles. Furthermore, the tool geometry results in a major difference between the cutting force acting on spherical cutting burrs and on end mills [21].

In view of those drawbacks, this paper puts forward a cortical bone milling force model based on the orthogonal cutting distribution method (OCDM) to calculate the equivalent milling force, so that the model can facilitate the application of force control in robotic orthopaedic surgery. In the OCDM, the transient milling is regarded as a combination of three orthogonal cutting operations. Based on the above combinations, the milling force coefficients are expressed by quadratic polynomials, which are used to indicate the change in milling force coefficients with the rotational angle. The bone milling force could be calculated by the milling force coefficients and milling parameters.

The paper is structured as follows. To begin with, the bone material properties are analyzed to comprehend the microstructure of the cortical bone, which is beneficial to explain the distribution of the orthogonal cutting forces. The orthogonal cutting of cortical bone is illustrated to obtain the three orthogonal cutting coefficients. Subsequently, the bone milling force model for cortical bone is established according to the tangential and normal components of the transient milling force during the slotting operation. Based on the OCDM, the transient cutting force coefficient is obtained through a quadratic polynomial, and it is affected by the feed direction and the dominant direction of osteons in bone materials. Then, the robotic bone milling force model is built considering the influence of robot arm processing. Next, an experimental platform is set up to simulate the bone milling process during robotic orthopedic surgery, and the force signals collected in the experiments are employed to verify the availability of the milling force model. Finally, the force model for bone milling satisfies the usage requirement in clinic orthopedic surgery, which promotes the development of force control in the robotic bone milling system.

2 OCDM-based bone milling force modeling

2.1 Related works

2.1.1 Analysis of bone material characteristics

The cortical bone is similar to a fiber-reinforced composite and has an anisotropic structure. In a microscopic view, the cortical bone mainly consists of osteons, cement line, and interstitial lamellae. Osteons are approximately cylindrical, 3–5 mm in length and 0.1–0.3 mm in diameter [22–24]. The cement line forms the boundary of the osteon, and the interstitial lamellae fills up the space between osteons. Similarly, the fiber-reinforced composite usually consists of fibers as reinforcing phases and polymers or metals as matrices. It is noted that the arrangement of osteons makes the cortical bone anisotropic. However, the fiber-reinforced composite hardly behaves anisotropically, as the forming process leads to disorder in the distribution of the reinforcing fibers. The directions of the bone materials are defined as parallel, cross, and transverse, based on the axial direction of osteons. Micrographs of cortical bone in different directions are presented in Fig. 1; the micrograph in the cross direction is similar to that in the parallel direction (not shown).
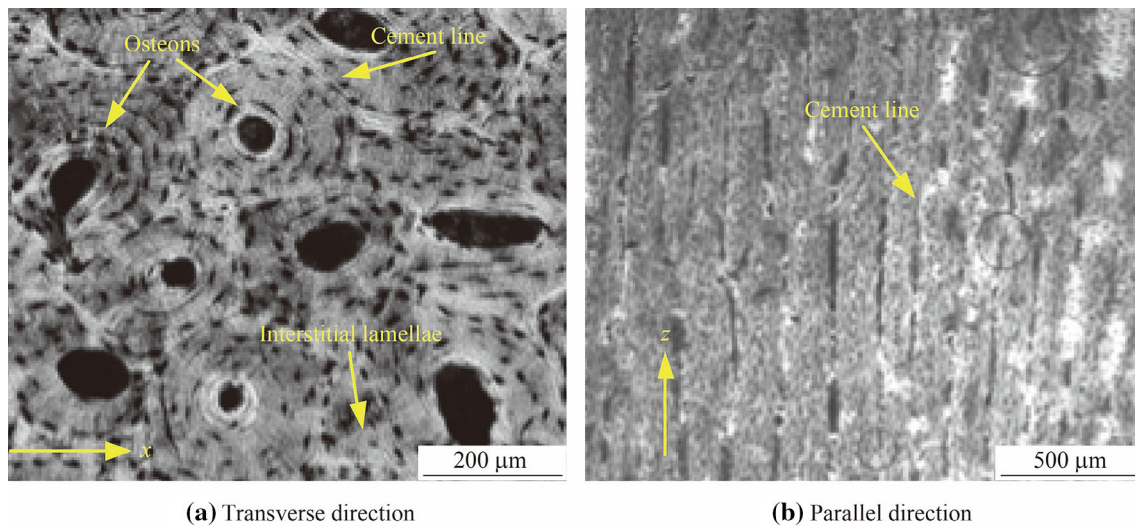
(a) Transverse direction

(b) Parallel direction

Fig. 1 Micrographs of cortical bone in different directions [25]

2.1.2 Orthogonal cutting force coefficients k_{para}, k_{cros}, k_{tran}

The three orthogonal cutting force coefficients could be obtained by the experimental data of the orthogonal bone cutting, corresponding to the directions of bone materials. The orthogonal cutting operations of cortical bone in three orthogonal directions are illustrated in Fig. 2. The cutting force in each orthogonal operation can be determined by the product of an empirical coefficient and the cutting area, and the coefficients are referred to as the cutting force coefficients, k_{para}, k_{cros} and k_{tran}, respectively linked to the parallel, cross, and transverse directions. According to the orthogonal cutting experimental results in Ref. [26], the order of the magnitudes of the cutting force coefficients is clearly shown as $k_{tran} > k_{para} > k_{cros}$. The three cutting force coefficients can be used to calculate the milling force in the feed direction during the bone machining process.

2.2 Bone milling process

The transient milling force $F(\theta)$ acting on the blade of the tool would change with the feed direction and the rotational angle, and it is expressed in Fig. 3. The x-axis in the tool coordinate frame is along the feed direction. The z-axis is set to coincide with the axis of the milling tool. $F_x(\theta)$ indicates the component of the transient milling force in the x direction dependent on the rotational angle, θ, and $F_y(\theta)$ represents the component of the transient milling force in the y direction dependent on the rotational angle, θ. Similarly, $F_t(\theta)$ and $F_n(\theta)$ denote the tangential and normal components of the transient milling force $F(\theta)$, respectively, and the force angle β between $F(\theta)$ and $F_n(\theta)$ is indicated.

The distribution of the transient bone milling force is beneficial to establish a direct relationship with the orthogonal cutting allocation, so that the transient milling force could be calculated based on the distribution of the cutting force coefficient. The following assumptions are made: (i) The bone material is simplified as an anisotropic material ignoring its heterogeneous property, and the diameter and length of the osteons are assumed to be constant. (ii) The thermal effect on the bone material characteristics is not taken into consideration in bone milling given that the machining condition hardly results in
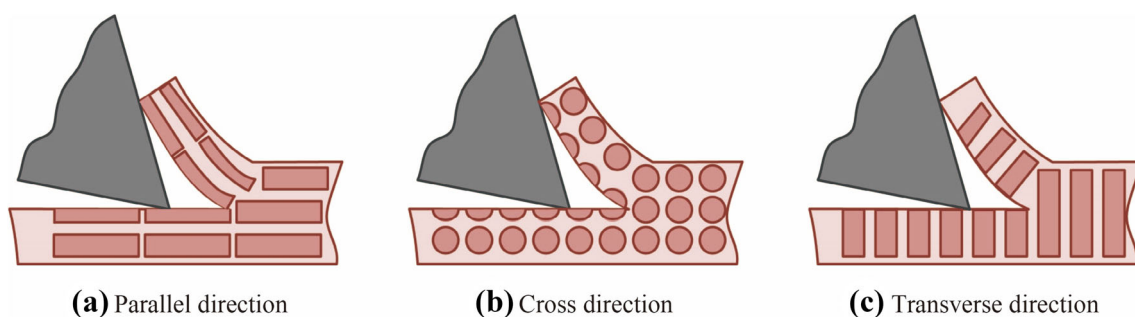

(a) Parallel direction

(b) Cross direction

(c) Transverse direction

Fig. 2 Orthogonal cutting operations in three cutting directions [26]
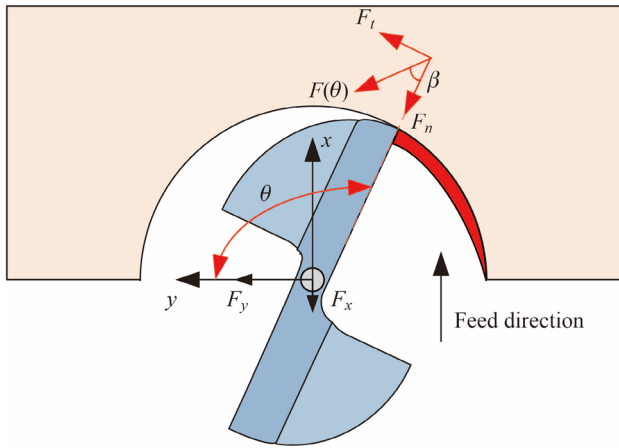
Fig. 3 Distribution situation of dynamic bone milling force for slotting

severe thermal damage. (iii) The milling force coefficients may be viewed as a variable independent of the cutting thickness, as the cutting thickness is small and barely changes during robotic bone milling operations. Furthermore, the cutting coefficients are assumed to change very little with cutting time. The bone materials would not lead to severe tool wear in milling, although tool wear could cause the cutting coefficients to change with cutting time [27].

2.2.1 Tangential and normal components F_t and F_n

The tangential and normal components of the transient milling force could be easily obtained according to the cutting force coefficients and the uncut chip area. The force angle, β, depends on the bone material and tool geometry and could determine the relationship between the tangential component $F_t(\theta)$ and the normal component $F_n(\theta)$. Accordingly, the tangential and normal components $F_t(\theta)$ and $F_n(\theta)$ can be expressed as

$$F_t(\theta) = k_{\text{mill\_t}}(\theta)bh, \tag{1}$$

$$F_n(\theta) = \frac{F_t}{\tan\beta}, \tag{2}$$

where b (m) represents the cutting width, h (m) the cutting thickness dependent on the rotational angle, θ (rad), and $k_{\text{mill\_t}}$ the general term of milling force coefficient in the tangential direction in a coordinate frame that rotates with the tool.

Besides, neglecting the z direction component, the x and y direction force components of the dynamic milling force, F_x and F_y, could be obtained as follows

$$F_x(\theta) = F_t\cos(\theta) + F_n\sin(\theta), \tag{3}$$

$$F_y(\theta) = F_t\sin(\theta) - F_n\cos(\theta). \tag{4}$$

2.2.2 Cutting thickness h

The cutting thickness of bone milling is related to the tool geometry and milling parameters. The transient milling of a single edge milling cutter could be analyzed during the milling process. The blade trajectory is approximated to a circular tool path when the tool rotates during translation [28, 29]. The feed per tooth, f_t, could be used to determine the maximum of cutting thickness. Meanwhile, the cutting thickness would be changed with the angle of rotation. The cutting thickness during bone milling could be obtained as

$$f_t = \frac{f}{\Omega N_t}, \tag{5}$$

$$h = f_t\sin(\theta), \tag{6}$$

where f represents the feed rate during the bone milling process (m/r); Ω is defined as the rotational speed of the spindle motor fixed on the end of the robot (r/s), and N_t indicates the number of teeth on the milling tool.

2.2.3 Cutting width b

The cutting width is determined by both the axial depth of cut, b_0, and the helix angle, γ, according to the geometric relationships between the tool and the chip during bone milling operations. Therefore, the cutting width, b (m), can be expressed as

$$b = \frac{b_0}{\cos(\gamma)}. \tag{7}$$

2.2.4 Bone milling force calculation

The effective milling force F is the resultant force in the x and y directions during the slotting cut, ignoring the acting force in the z direction. Meanwhile, F is also expressed using $F_t(\theta)$ and $F_n(\theta)$. Furthermore, the start angle for slotting is $\theta_s = 0$, while the exit angle is defined as $\theta_e = \pi$. Thus, the bone milling force is obtained as

$$F = \frac{\int_0^\pi \sqrt{F_x^2 + F_y^2}\,d\theta}{\pi} = \frac{\int_0^\pi \sqrt{F_t^2 + F_n^2}\,d\theta}{\pi}, \tag{8}$$

where F represents the effective value of the total acting force during the bone milling process.

2.3 OCDM-based robotic milling force model

2.3.1 OCDM

The OCDM regards the bone milling form at a certain time as a combination of several specific orthogonal cuttings

and indicates the distribution situation by the distribution effect function $k_{mill\_t}(\theta)$ linked with the orthogonal cutting coefficients k_{para}, k_{cros} and k_{tran}. According to the above combinations, the milling force coefficients can be expressed by parabolic functions. The bone milling force could be obtained based on the milling force coefficients and milling parameters by Eq. (8).

In one cycle of bone milling, the milling process could be regarded as the mutual transformation of orthogonal cutting forms. Meanwhile, the tangential component of the transient milling force coefficient, k_{mill_t}, varies between the orthogonal cutting force coefficients, and the change in milling force coefficient in a rotating period is expressed by a polynomial [6]. For simplifying the calculation operations, a quadratic polynomial is selected to fit the change in milling force coefficient with the rotational angle. Thus, k_{mill_t} could be represented through a quadratic polynomial. Furthermore, the corresponding quadratic polynomial can be uniquely determined by the known value of k_{mill_t} at the specific rotational angle, θ, and can be expressed as

$$k_{mill\_t}(\theta) = a\theta^2 + b\theta + c, \tag{9}$$

where a, b and c could be determined by the orthogonal cutting coefficients in different feed directions.

According to the relative location relationship between the feed direction and the directions of bone materials, the three milling processes could be easily identified in Fig. 4.

The three bone milling force cases are analyzed, and the distribution functions $k_{mill\_t}(\theta)$ in the three feed directions are expressed as $k_{mill\_pt}(\theta)$, $k_{mill\_ct}(\theta)$ and $k_{mill\_tt}(\theta)$.

2.3.2 $k_{mill\_pt}(\theta)$ in the parallel feed direction

The end milling process in the parallel direction could be considered as the combination of orthogonal cutting in the transverse and parallel directions, as shown in Fig. 5, and the transverse orthogonal direction cutting is the major cutting operation during the bone milling process. The transient milling in the parallel feed direction is similar to the orthogonal cutting in the parallel direction when the rotational angle is 0 or π, so that $k_{mill\_pt}(0)$ or $k_{mill\_pt}(\pi)$ equals k_{para}. The transient milling in the parallel feed direction is similar to the orthogonal cutting in the transverse direction when the rotational angle is 0.5π, so that $k_{mill\_pt}(0.5\pi)$ equals k_{tran}, as indicated in Fig. 6a. Based on the OCDM, the parabolic coefficients of parallel milling can be calculated according to the known cutting force coefficients of three rotational angles, and the distribution function, $k_{mill\_pt}(\theta)$, could be expressed as

$$k_{mill\_pt}(\theta) = -\frac{4}{\pi^2}(k_{tran} - k_{para})\theta^2 + \frac{4}{\pi}(k_{tran} - k_{para})\theta + k_{para},$$

$$\tag{10}$$

(a) Parallel direction   **(b)** Cross direction   **(c)** Transverse direction
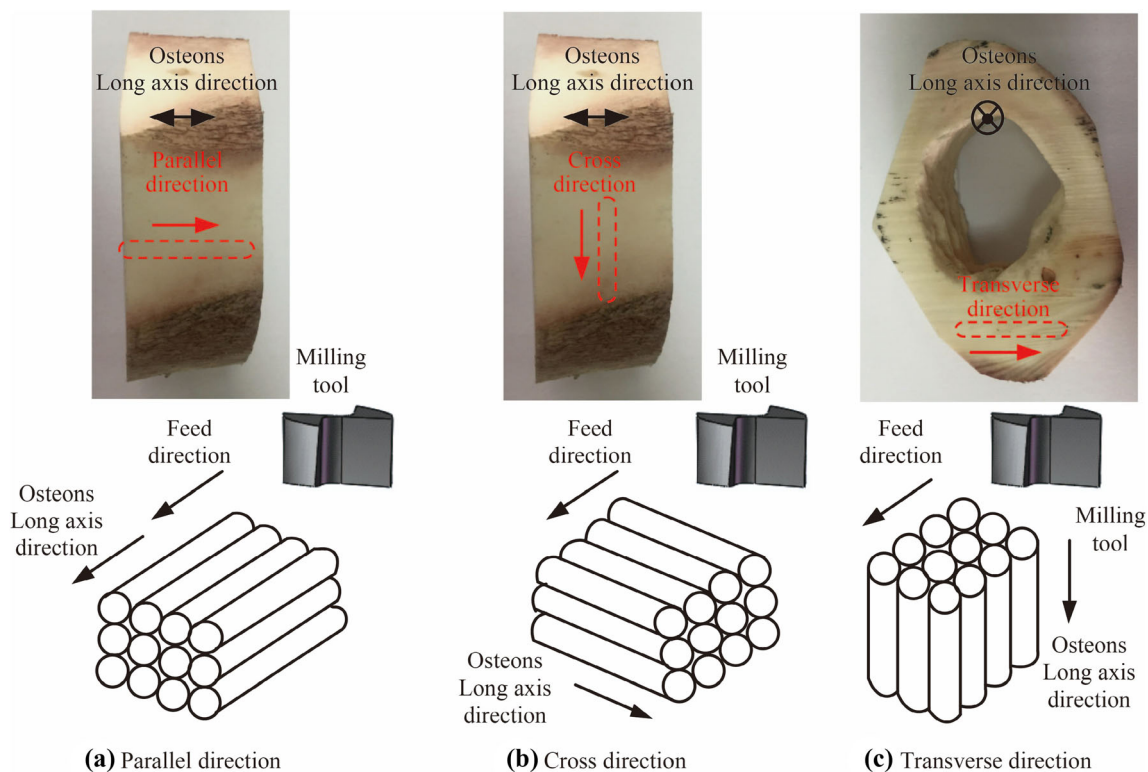
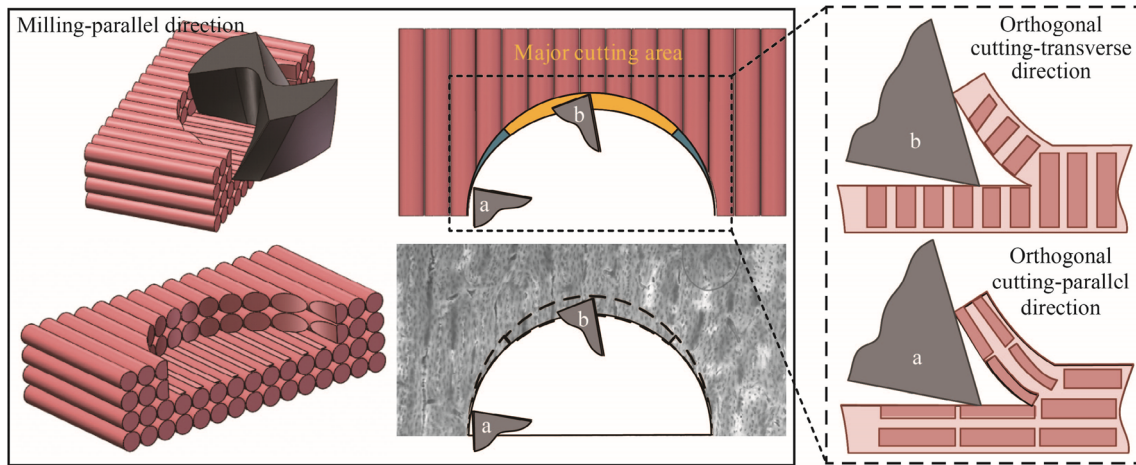Fig. 4 Bone milling processes in three cutting directions

Fig. 5 Schematic diagram of the milling process in parallel direction
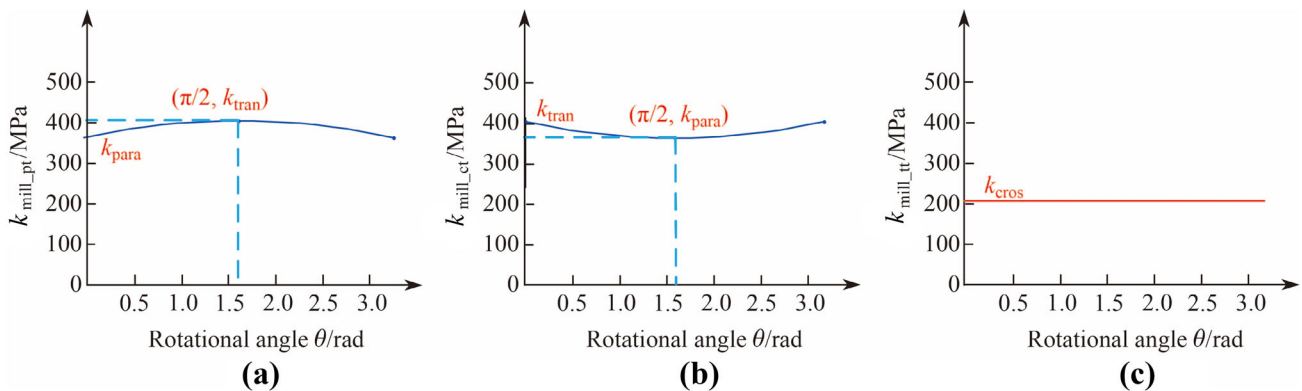

Fig. 6 Tangential component of bone milling force coefficients in the three feed directions **a** the distribution function, $k_{\mathrm{mill\_pt}}(\theta)$, in the parallel feed direction, **b** the distribution function, $k_{\mathrm{mill\_ct}}(\theta)$, in the cross feed direction, **c** the distribution function, $k_{\mathrm{mill\_tt}}(\theta)$, in the transverse feed direction

where θ is defined as the rotation angle of the milling cutter blade (rad), and the value is zero when the blade has just been cut into the bone samples. The feed direction is defined along the x-axis in the tool coordinate frame. The z-axis is set to coincide with the axis of the milling tool.

2.3.3 $k_{\mathrm{mill\_ct}}(\theta)$ in the cross feed direction

The end milling behavior in the cross direction is regarded as the combination of orthogonal cutting forms in the parallel and transverse directions, as shown in Fig. 7, and the parallel orthogonal cutting operation is kept in the major position. The transient milling in the cross feed direction is similar to the orthogonal cutting in the transverse direction when the rotational angle is 0 or π, so that $k_{\mathrm{mill\_pt}}(0)$ or $k_{\mathrm{mill\_pt}}(\pi)$ equals k_{tran}. The transient milling in the parallel feed direction is similar to the orthogonal cutting in the parallel direction when the rotational angle is 0.5π, so that $k_{\mathrm{mill\_pt}}(0.5\pi)$ equals k_{para}, as indicated in

Fig. 6b. Based on the OCDM, the parabolic coefficients of cross milling can be obtained according to the known cutting force coefficients of three rotational angles, and the distribution function, $k_{\mathrm{mill\_ct}}(\theta)$, could be expressed as

$$k_{\mathrm{mill\_ct}}(\theta) = -\frac{4}{\pi^2}(k_{\mathrm{para}} - k_{\mathrm{tran}})\theta^2 + \frac{4}{\pi}(k_{\mathrm{para}} - k_{\mathrm{tran}})\theta + k_{\mathrm{tran}},$$

(11)

where the tool coordinate frame of the milling in the cross direction is defined similarly to that in the parallel direction.

2.3.4 $k_{\mathrm{mill\_tt}}(\theta)$ in the transverse feed direction

The milling force coefficient in the transverse direction, $k_{\mathrm{mill\_tt}}(\theta)$, is largely different from the above two, as shown in Fig. 8. The end milling operation in the transverse direction can be equivalent to the orthogonal cutting in the
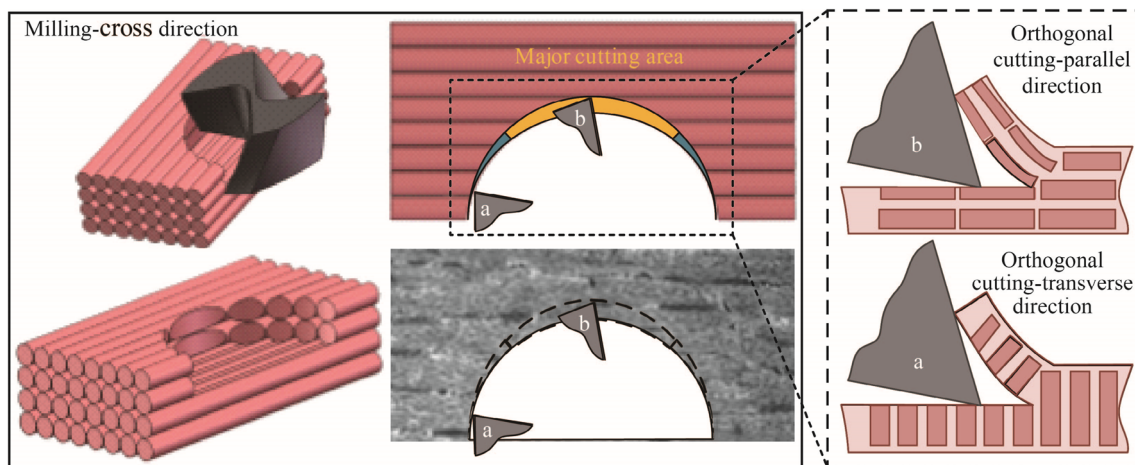
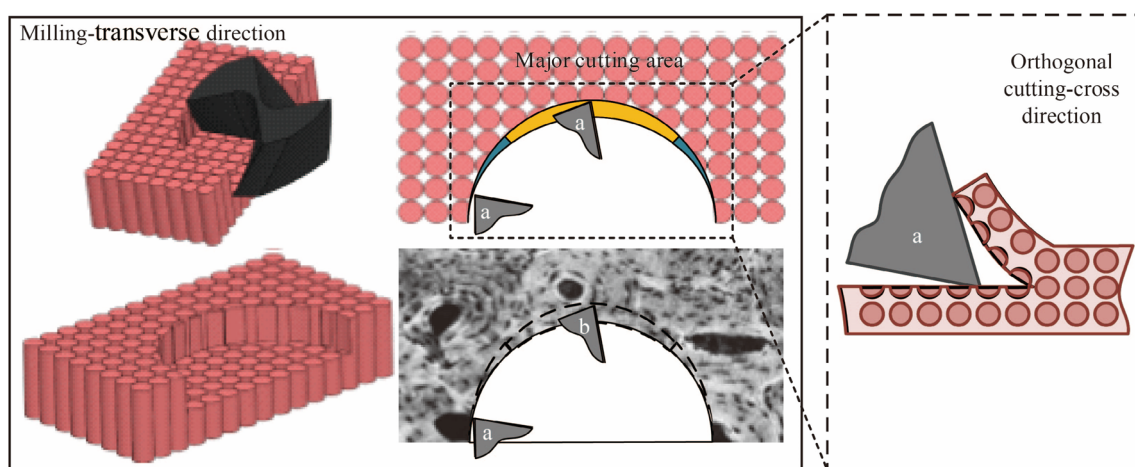**Fig. 7** Schematic diagram of the milling process in cross direction

Fig. 8 Schematic diagram of the milling process in transverse direction

cross direction, so that $k_{\mathrm{mill\_tt}}(\theta)$ keeps unchanged, as shown in Fig. 6c. Thus, $k_{\mathrm{mill\_tt}}(\theta)$ could be calculated as

$$k_{\mathrm{mill\_tt}}(\theta) = k_{\mathrm{cros}}, \tag{12}$$

where the tool coordinate system is set similar to that in the parallel or cross direction.

2.3.5 Robotic bone milling force modeling

The effect of robotic milling on the milling force is different from that of machine tool processing owing to the low structural stiffness and fixing method of the force sensor. The robot arm has significantly less stiffness, which would have an influence on the milling force [30, 31]. The low stiffness tends to lead to chatter of the structure during bone milling operations, and the chatter has the specified amplification effect for the input signal of the milling force when the processing continues at a stable spindle speed. In view of the milling vibration stripes on the machining

surface of bone materials, it is clear that chatter occurs during robotic bone milling operations, and it is often the case that bone milling can still be performed when low-amplitude chatter occurs. However, chatter with a low amplitude can increase the amplitude of bone milling forces.

The bone milling forces acting on the tool tip are transferred on the robotic force sensor, and the structural chatter and fixing method of the force sensor have an amplification effect. The milling forces acting on the tip are regarded as the input of the milling system, and the force signals measured by the force sensor are the output of the milling system. The relationship between the input and output is expressed by a transfer function. The amplitude of the transfer function determines the gain effect of the robotic milling force. Moreover, the gain effect can be obtained by the frequency response function test method. Thus, the robotic bone milling force model is defined as

$$F_{\mathrm{m}} = \lambda F, \tag{13}$$

where F_{m} is defined as the milling force obtained by the force sensor during robotic bone milling and λ represents the gain coefficient of the robotic milling system.

3 Experimental study

3.1 Experimental platform

A test platform is built to verify the feasibility of the mechanism analysis and influence on the milling force in different bone milling directions, as shown in Fig. 9. The ABB IRB1200 industrial robot arm is employed to carry out specific actions with position precision of 0.05 mm and repositioning precision of 0.02 mm. The force sensor, mounted on the end flange of the robot, could collect the signals of cutting forces and torques, and the Test Signal Viewer software can be specially applied to extract and display the signal collected by the force sensor at the sampling rate of 1 984 Hz. The GDZ48-300 water-cooled motorized spindle is fixed on the force sensor, with a maximum speed of 60 000 r/min. The ACD200-2S inverter can flexibly adjust the speed of the spindle motor. A two-blade medical stainless-steel end milling cutter is employed to perform the milling task and a diameter of 2 mm is selected. The prepared bone specimen is fixed on special fixtures.

3.2 Bone specimen

Bovine bone is selected as the experimental material to simulate human bone during milling experiments given their similar mechanical characteristics and chemistry compositions [32]. Fresh bovine femurs were purchased from a local butcher and were stored at $-20\ ^\circ\mathrm{C}$ in a refrigerator [21, 33, 34]. The diaphysis of the bovine femur, mainly consisting of cortical bone, was seen into several bone blocks with the same size. Next, the bone blocks were roughly machined by the UNIPOL-810 polishing machine with a 80 grit diamond grinding disc, and then polished with a diamond grinding disc of 1 200 grit to form the bone samples with the machined planes, as shown in Fig. 10. Afterwards, the prepared bone samples were placed in the refrigerator at $-20\ ^\circ\mathrm{C}$ for preservation. Within an hour before the experiment, the bone specimen was taken out from the refrigerator and immersed in normal saline at room temperature to restore the mechanical behavior of the bone material.

3.3 Experimental validation

The effect of feed direction on the milling force for robotic bone operations could be verified by an analysis of the experimental results and milling force prediction, and the comparisons between the test data and theoretical calculation also show the rationality of the cutting mechanism analysis for a bone milling process.

3.3.1 Experiment operations

The robot arm performs the slotting task in a constant direction, while the force measured by the sensor is recorded on a computer. The milling operations in the three standard directions are finished by changing the position and orientation of the bone sample. The dynamic force information in the three directions of the machining coordinate axes is collected by the force sensor at the sampling period of 0.504 ms. A series of milling tests are carried out under different spindle speeds (9 000–15 000 r/min), feed rates (3–5 mm/s), and cutting depth (0.5 and 1 mm), so that the experimental results could be utilized to verify the
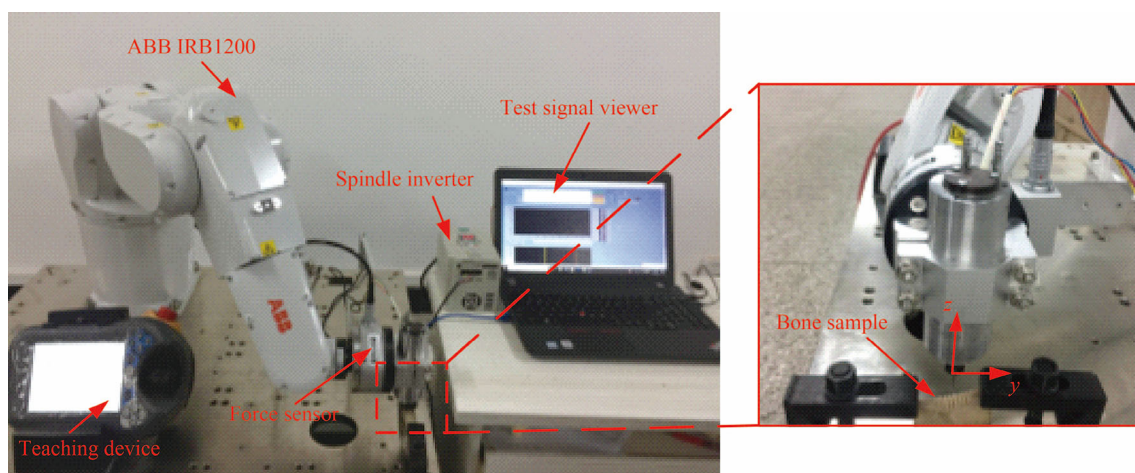

Fig. 9 Experiment setup of robotic bone milling for force measurement
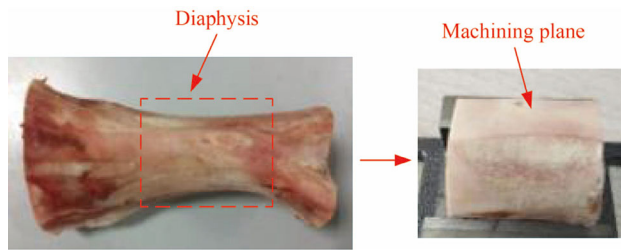
Fig. 10 Bone specimen preparation

robustness of the proposed model. The bone milling parameters were selected from the clinical experience for balancing the machining force and efficiency, as presented in Table 1.

3.3.2 Analysis of experimental result

The force signals in different milling directions were measured by the force sensor. For evaluating the milling force, the resultant force in the sensor coordinate system, F_{me}, can be written as

$$F_{me} = \sqrt{F_{x0}^2 + F_{y0}^2 + F_{z0}^2}, \qquad (14)$$

where the forces in three axial directions of the sensor coordinate frame are expressed as F_{x0}, F_{y0}, and F_{z0}. The average values of the milling total forces in different machining directions are indicated in Fig. 11. The average value refers to an average of the resultant force on the time scale, and it provides a comprehensive characterization of the resultant force magnitude in different machining directions.

3.3.3 Prediction of robotic milling force F_{rm}

The milling force could be predicted according to the milling parameters in the experiment. The gain coefficient of the milling system is obtained in the frequency response function tests. If the input of the milling system is a harmonic signal, the output is also a harmonic signal. In the steady state, the amplitude ratio of the output signal to the input signal is the gain coefficient of the system. The JZK-10 shaker provides the harmonic exciting force as the input of the milling system, and the frequency of the exciting force is equal to the rotation frequency in bone milling. When the spindle speed is 1 200 r/min, the exciting frequency is set as 200 Hz. The cutting force coefficients are obtained based on a large number of orthogonal cutting tests, and the orthogonal cutting force coefficients can be determined based on Ref. [26], i.e., $k_{para} = 364$ MPa, $k_{cros} = 210$ MPa, and $k_{tran} = 405$ MPa. According to the force calculation method for robotic bone milling, the verification results of the bone milling force are presented in Table 1.

It can be observed from Table 1 that the theoretical prediction values of effective milling forces in different directions stay within the range of the measured values, and thus, the prediction values can represent the magnitude of the measured values. Therefore, the force prediction for robotic bone milling can satisfy the requirements of

Table 1 Verification results of milling force for robotic bone operations in different feed directions

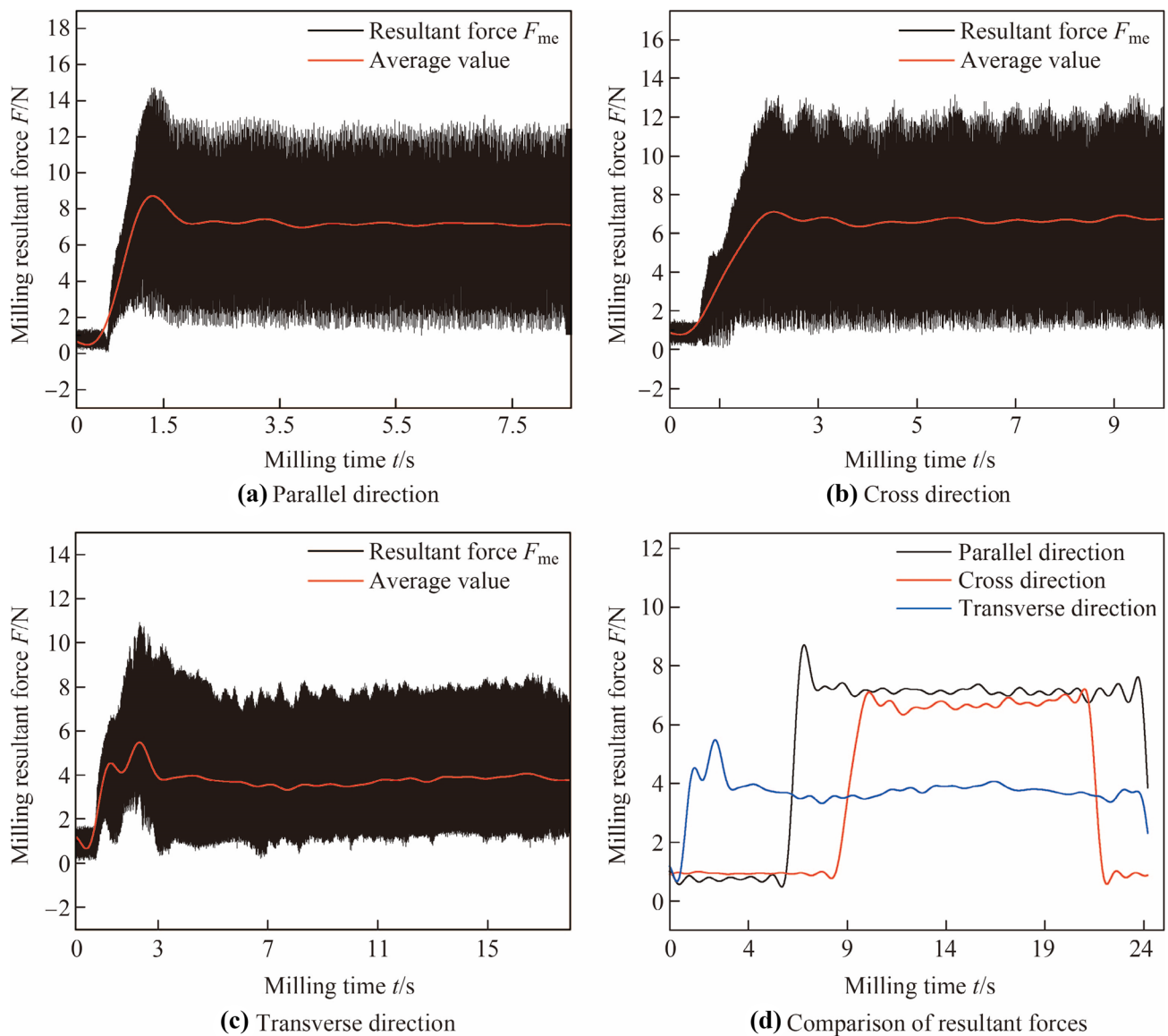| No.	Spindle speed Ω/ (r·min^{-1})	Feed rate v_f / (mm·s^{-1})	Cutting depth b/ mm	Gain coefficient λ	Milling directions	Robotic milling force F_{rm}/N	
						Measured value	Theoretical value
1	9 000	5	1	1.25	Parallel	6.77–7.42	7.11
					Cross	6.36–7.13	6.74
					Transverse	3.32–4.07	3.78
2	12 000	3	1	1.25	Parallel	2.86–3.64	3.20
					Cross	2.65–3.28	3.03
					Transverse	1.46–2.09	1.70
3	15 000	4	0.5	1.25	Parallel	1.38–2.07	1.71
					Cross	1.27–2.03	1.62
					Transverse	0.79–1.27	0.91

Fig. 11 Resultant forces in different milling directions

orthopedic surgery, and the influences of milling directions on the milling force have also proved to be reasonable.

4 Conclusions

In this paper, a cortical bone milling force model based on the OCDM is presented. The bone milling force in different feed directions can be predicted, which reasonably explains the effect of feed directions on the milling force during robotic bone operations. The OCDM is employed to analyze the transient milling force in bone milling for the first time. The experimental observations indicate that the OCDM can be utilized to predict the bone milling force. The milling force in parallel or cross direction is obviously higher than that in the transverse direction during robotic milling of a cortical bone. The encouraging results verify the rationality of the proposed bone milling force model. The bone milling force model presented in this paper will be helpful to promote the development of force control in bone machining.

References

1. Jacobs CH, Pope MH, Berry JT et al (1974) A study of the bone machining process-orthogonal cutting. J Biomech 7(2):131–136
2. Jacob CH, Berry JT, Pope MH et al (1976) A study of the bone machining process-drilling. J Biomech 9(5):343–349
3. Sui J, Sugita N, Ishii K et al (2013) Force analysis of orthogonal cutting of bovine cortical bone. Mach Sci Technol 17(4):637–649
4. Ong FR, Bouazza-Marouf K (1999) The detection of drill bit break-through for the enhancement of safety in mechatronic assisted orthopaedic drilling. Mechatronics 9(6):565–588
5. Sugita N, Osa T, Aoki R et al (2009) A new cutting method for bone based on its crack propagation characteristics. CIRP Ann 58(1):113–118
6. Yao Q, Luo M, Zhang D et al (2018) Identification of cutting force coefficients in machining process considering cutter vibration. Mech Syst Signal Process 103:39–59
7. Saito A, Takahashi M, Miyano Y et al (2014) Influence of the cutting condition on cutting performance with twisted fixed abrasive diamond saw wire (ADW). Int J Soc Mater Eng Resour 20(2):181–185
8. Liao Z, Axinte DA, Gao D (2017) A novel cutting tool design to avoid surface damage in bone machining. Int J Mach Tools Manuf 116:52–59
9. Feldmann A, Ganser P, Nolte L (2017) Orthogonal cutting of cortical bone: temperature elevation and fracture toughness. Int J Mach Tools Manuf 118:1–11
10. Santiuste C, Rodríguez-Millán M, Giner E et al (2014) The influence of anisotropy in numerical modeling of orthogonal cutting of cortical bone. Compos Struct 116:423–431
11. Wiggins KL, Malkin S (1978) Orthogonal machining of bone. J Biomech Eng 100(3):122–130
12. Sugita N, Mitsuishi M (2009) Specifications for machining the bovine cortical bone in relation to its microstructure. J Biomech 42(16):2826–2829
13. Alam K, Mitrofanov AV, Silberschmidt VV (2009) Finite element analysis of forces of plane cutting of cortical bone. Comput Mater Sci 46(3):738–743
14. Takabi B, Tai BL (2017) A review of cutting mechanics and modeling techniques for biological materials. Med Eng Phys 45:1–14
15. Lee JE, Gozen BA, Ozdoganlar OB (2012) Modeling and experimentation of bone drilling forces. J Biomech 45(6):1076–1083
16. Sui J, Sugita N, Ishii K et al (2014) Mechanistic modeling of bone-drilling process with experimental validation. J Mater Process Technol 214(4):1018–1026
17. Lughmani WA, Bouazza-Marouf K, Ashcroft I (2015) Drilling in cortical bone: a finite element model and experimental investigations. J Mech Behav Biomed Mater 42:32–42
18. Arbabtafti M, Moghaddam M, Nahvi A et al (2011) Physics-based Haptic simulation of bone machining. IEEE Trans Haptics 4(1):39–50
19. Al-Abdullah KIA, Abdi H, Lim CP et al (2018) Force and temperature modelling of bone milling using artificial neural networks. Measurement 116:25–37
20. Liao Z, Axinte D, Gao D (2019) On modelling of cutting force and temperature in bone milling. J Mater Process Technol 266:627–638
21. Mamedov A, Lazoglu I (2015) Micro ball-end milling of free-form titanium parts. Adv Manuf 3(4):263–268
22. Conward M, Samuel J (2016) Machining characteristics of the haversian and plexiform components of bovine cortical bone. J Mech Behav Biomed Mater 60:525–534
23. Yeager C, Nazari A, Arola D (2008) Machining of cortical bone: surface texture, surface integrity and cutting forces. Mach Sci Technol 12(1):100–118
24. Liao Z, Axinte DA (2016) On monitoring chip formation, penetration depth and cutting malfunctions in bone micro-drilling via acoustic emission. J Mater Process Technol 229:82–93
25. Griesmann U (2012) Microscopy of bone and step-by-step sample preparation. Micscape. http://www.microscopy-uk.org.uk/mag/artmay12/ug-Bone.html. Accessed 15 Oct 2018
26. Liao Z, Axinte DA (2016) On chip formation mechanism in orthogonal cutting of bone. Int J Mach Tools Manuf 102:41–55
27. Liu Y, Wang Z, Liu K et al (2017) Chatter stability prediction in milling using time-varying uncertainties. Int J Adv Manuf Technol 89(9/12):2627–2636
28. Kumanchik LM, Schmitz TL (2007) Improved analytical chip thickness model for milling. Precis Eng 31(3):317–324
29. Han X, Tang L (2015) Precise prediction of forces in milling circular corners. Int J Mach Tools Manuf 88:184–193
30. Kavina YB, Kochekali H, Whitaker RA (1987) An analytical and modular approach to robotic force control using a wrist-based force sensor. In: McGoldrick PF (ed) Advances in manufacturing technology II: proceedings of the third national conference on production research. Springer, Boston, pp 175–179
31. Cordes M, Hintze W, Altintas Y (2019) Chatter stability in robotic milling. Robot Comput Integr Manuf 55:11–18
32. Alam K, Mitrofanov AV, Silberschmidt VV (2011) Experimental investigations of forces and torque in conventional and ultra-sonically-assisted drilling of cortical bone. Med Eng Phys 33(2):234–239
33. Luczynski KW, Steiger-Thirsfeld A, Bernardi J et al (2015) Extracellular bone matrix exhibits hardening elastoplasticity and more than double cortical strength: Evidence from homogeneous compression of non-tapered single micron-sized pillars welded to a rigid substrate. J Mech Behav Biomed Mater 52:51–62
34. Walden SJ, Evans SL, Mulville J (2017) Changes in Vickers hardness during the decomposition of bone: Possibilities for forensic anthropology. J Mech Behav Biomed Mater 65:672–678

Qi-Sen Chen graduated from Northeast University in 2020 with a master's degree. Main research direction is bone milling force, milling temperature diffusion mechanism, etc.

Li Dai is a lecturer in the Institute of Mechanical Electronics, School of Mechanical Engineering and Automation, Northeastern University. She obtained a doctor's degree from Northeast University in 2008. Main research direction is artificial intelligence, system dynamics, mechatronics, etc.
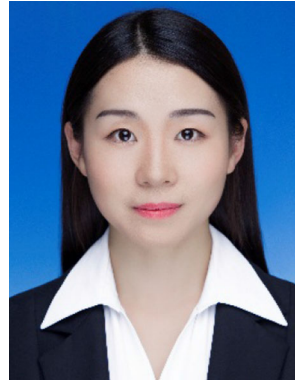
Qiu-Xiang Shi graduated from Northeast University in 2019 with a master's degree. Main research direction is bone milling, surface quality of bone cutting, etc.

Yu Liu is an associate professor and doctor advisor in the school of Mechanical Engineering & Automation, Northeastern University in China. His major research directions are mechanical structure and system dynamics, robotic bone milling.